Turkish Journal of Civil Engineering, 2024 71-94, Paper 770, ***Research Article***

Energy-Based Assessment of Liquefaction Behavior of a Non-Plastic Silt Based on Cyclic Triaxial Tests

Alper SEZER[1]
Çağlar KUMAŞDERE[2]
Nazar TANRINIAN[3]
Eyyüb KARAKAN[4*]

ABSTRACT

Earthquakes cause cyclic shear deformations in soil and build-up of excessive pore water pressure as a result of undrained loading, accompanied with rearrangement of soil particles and degradation in stiffness of the soil due to decrease in effective stresses. During loading, the onset of soil liquefaction is defined as a stress state in which the excess pore water pressure is equalized to the total stress. From this point of view, assessment of the pore water pressure development pattern under cyclic loading has been one of the most salient research topics in geotechnical and earthquake engineering. In this study, results of a series of cyclic triaxial tests on non-plastic silt specimens consolidated under 100 kPa effective isotropic consolidation pressure were used to question the modelling ability of pore pressure development models previously proposed for sands. Tests were performed on specimens of 6 different initial relative densities (D_r) ranging between 30-80% and 10 different cyclic stress ratios (CSR). The key parameters of pore water pressure development and shear deformation in the energy-based model used are relative density, cyclic stress ratio and number of cycles. The results revealed that, these energy-based models have a strong potential in evaluation of pore water pressure development pattern of non-plastic silts. Test results also show that the increase in relative density and decrease in CSR causes a ladderlike behavior among pore water pressure and cyclic shear strain, which is relevantly rendered by energy-based models.

Keywords: Pore water pressure, silt, cyclic triaxial tests, energy-based models.

Note:
- This paper was received on April 17, 2023 and accepted for publication by the Editorial Board on December 22, 2023.
- Discussions on this paper will be accepted by July 31, 2024.

• https://doi.org/10.18400/tjce.1283189

1 Ege University, Department of Civil Engineering, Izmir, Türkiye
alper.sezer@ege.edu.tr - https://orcid.org/0000-0002-2663-2028

2 Ege University, Department of Civil Engineering, Izmir, Türkiye
caglar.kumasdere@gmail.com - https://orcid.org/0000-0003-2133-6796

3 DNV France Sarl, Paris, France
ntanrinian@gmail.com - https://orcid.org/0000-0002-5929-0757

4 Kilis 7 Aralik University, Department of Civil Engineering, Kilis, Türkiye
eyyubkarakan@kilis.edu.tr - https://orcid.org/0000-0003-2133-6796

* Corresponding author

1. INTRODUCTION

It is a well-known fact that, during earthquake loading, soils may completely lose their strength and imitate the viscous behavior of a "liquid". Identified as liquefaction, this phenomenon is one of the reasons causing severe damage during seismic action. Many liquefaction cases were reported in the past, particularly in San Francisco (1906), Alaska (1964), Niigata (1964), San Fernando (1971), Kocaeli (1999) as reported in literature [1]. Evaluation of the pore water pressure development mechanisms triggering liquefaction has become one of the most important and interesting topics in geotechnical earthquake engineering [1]. Liquefaction leads to loss of shear strength caused by the build-up of excessive pore water pressure. Liquefaction can cause loss of bearing capacity, floating of buried structures, ground subsidence, settlement of embankments, lateral displacement of slopes and retaining walls [2-3].

Excess pore pressures in a soil during cyclic loading can be divided into two components, transient and residual. Transient pore water pressures in saturated soils occur due to changes in the applied average normal stresses resulting from dynamic loading [4-5]. Since the resulting pore water pressures are equal to the change in the total stress acting on the soil, transient excess pore pressures will have an inconsiderable effect on the effective stresses acting on the soil. Conversely, residual pore water pressures result from gradual collapse of the soil skeleton (i.e. plastic deformations) and therefore change the effective stresses acting on the soil. As a result, residual pore water pressures directly affect the strength and stiffness of the soil. During stress controlled cyclic tests, the residual pore pressures are those that are present when the applied deviator stress equals to (or exceeds) zero [6-7]. Residual pore pressures are often measured as the residual pore water pressure ratio. Pore water pressure ratio (r_u) defined as the ratio of the residual pore water pressure (u_{xs}) to the initial effective confining stress (σ'_o) acting on the soil. This ratio ranges from zero (i.e. no residual pore pressure) to one (i.e. complete transfer of load to pore water or "liquefaction") and thus provides more information than just the magnitude of the residual pore pressure.

In the literature, much effort is given on understanding the cyclic pore water pressure development pattern; these can be classified as stress-based [8,9], deformation-based [10, 11], energy-based [7, 12], and plasticity-based [13] models.

Four stress-based models can be used to predict pore water pressure generation for a non-plastic silt subjected to dynamic loading. The first model was developed by the empirical solution of Seed et al. [8]. In the sequel, a simplified alternative model was proposed by Booker et al. [9]. Three decades later, Polito et al. [14] revisited the method proposed by Seed et al. [1] with the help of statistics. Lastly, Baziar et al. [15] proposed an alternative closed form solution for silts using statistical software based on Seed et al.'s [8] methodology.

An empirical model considering excess pore-water pressure ratio (r_u) and ratio of number of cycles to liquefaction (N/N_{liq}) was suggested by Lee and Albaisa [16]. Seed et al. [8] proposed an empirical formula as given in Equation (1) based on data from De Alba et al. [17]:

$$R_u = \frac{1}{2} + \frac{1}{\pi} * \arcsin\left[2 * \left(\frac{N}{N_{liq}}\right)^{\frac{1}{\alpha}} - 1\right] \quad (1)$$

where α is a function of soil properties and testing conditions (α=0.7; and N=number of equivalent uniform loading cycles). Recently, Polito et al. [14] revised Seed et al.'s [8] method by use of statistical approaches and suggested that the model coefficient alpha (α) is dependent on several factors including cyclic stress ratio (CSR), fines content (FC), and relative density (D_r):

$$\alpha = 0.01166 * FC + 0.007397 * D_r + 0.01034 * CSR + 0.5058 \quad (2)$$

Equation (2) is valid for coarse grained soils with fines content (FC) less than 35%. For clean sands (FC=0), the effect of CSR on results is relatively insignificant, and it is evident that relative density has a remarkable effect on α. It is estimated that α should be between 0.73 to 1.14 [3]. Seed et al. [8] developed an empirical equation for assessment of excess pore-water pressure ratio (r_u) as a function of cycle ratio. This expression was subsequently simplified by Booker et al. [9] and is given as:

$$R_u = \frac{2}{\pi} arcsin\left[\left(\frac{N}{N_{liq}}\right)^{\frac{1}{2\alpha}}\right] \quad (3)$$

Equation (3) is composed of two calibration parameters, namely, number of cycles to liquefaction (N_{liq}) and empirical constant (α), which is to be determined by stress-controlled testing. For a certain soil, N_{liq} increases with increasing relative density (D_r) and decreases with increasing cyclic stress ratio (CSR); α is a constant-a function of soil type and test conditions. Baziar et al. [15] proposed the correlation given in Equation (4) based on model of Booker et al. [9]:

$$R_u = \frac{2}{\pi} arcsin\left[\left(\frac{N}{N_{liq}}\right)^{\frac{1}{2\alpha}}\right] + \sqrt[\beta]{\left(1 - \left(2 * \frac{N}{N_{liq}} - 1\right)^2\right)} \quad (4)$$

In Equation 4, α and β are two constants which are identified for different types of soils based on their silt content.

Early efforts on evaluation of dynamic characteristics of soil utilize slow and rapid transient loading on soil specimens by impact loading on a spring [18]. However, cyclic triaxial testing by analysis of stress reversals for assessment of liquefaction susceptibility and dynamic characteristics of soils were introduced by studies of Seed & Fead [19] and Seed [20]. During the past decade the test device, thanks to developments of data acquisition and measurement technology, use of the test has steadily increased, and it has been the most commonly used laboratory test for evaluating dynamic response of soils. The test has even broadened its use to analysis of response of foundations of offshore structures. However, sometimes, the difficulties in obtaining undisturbed specimens, imitation of loading and stress conditions come up with the need of modeling efforts. In this regard, an empirical energy-based excess pore pressure generation model has been developed that accurately approximates residual pore pressure generation in cohesionless soils under stress-controlled cyclic loading. The energy-based model has a simple mathematical form and a single calibration parameter (PEC), which facilitates its implementation and calibration.

Energy based pore water pressure development models are beneficial for understanding the pore water pressure development pattern during seismic loading. Some researchers developed models considering deformation energy and established relationships among change in excess pore pressure and energy absorbed per unit soil volume for a certain loading cycle [21]. They proposed an equation establishing a relationship between the volume change of dry sand and pore water pressure, considering an energy-based model. Further attempts were based on theoretical studies, mainly focusing on developing experimental models using empirical data [22-28]. A comprehensive summary of previous studies is presented by Green [28] along with a new set of calibration parameters. Additionally, Green et al. [7] presented a compilation of previous studies along with a new set of calibration parameters. The following model is proposed by Green et al. [7]:

$$r_u = \sqrt{\frac{W_s}{PEC}} \leq 1 \tag{5}$$

Here; W_s is the energy dissipated per unit volume of soil divided by initial effective confining pressure and PEC is the Pseudo Energy Capacity, which is a calibration parameter. An infinitesimal increase in W_s can be linked to state of stress and changes in strain (Equations 6 and 7).

$$dW_s = \frac{(\sigma'_v\, d\varepsilon_v + 2\sigma'_h\, d\varepsilon_h + \tau_{vh}\, d\gamma_{vh} + \tau_{hv}\, d\gamma_{hv})}{\sigma'_{m0}} \tag{6}$$

where; dW_s is the dissipated energy increase normalized by the initial mean effective stress; σ'_{m0} is the initial mean effective stress; $\boldsymbol{\sigma'_v}$ is the vertical effective stress; $\mathbf{d\varepsilon_v}$ is the change in vertical strain; $\boldsymbol{\sigma'_h}$ is the horizontal effective stress; $\mathbf{d\varepsilon_h}$ is the change in radial strain; $\boldsymbol{\tau_{vh}}$ is the horizontal shear stress acting on a plane with a vertical normal; $\mathbf{d\gamma_{vh}}$ is the change in shear strain due to change in τ_{vh}; $\boldsymbol{\tau_{hv}}$ is the vertical shear stress acting on a plane with a horizontal normal and $\mathbf{d\gamma_{hv}}$ is the change in shear strain due to change in $\boldsymbol{\tau_{hv}}$;

$$W_s = \frac{1}{2\sigma'_0}\sum_{i=1}^{n-1}\left[\left(\sigma_{d,i+1} + \sigma_{d,i}\right).\left(\varepsilon_{a,i+1} - \varepsilon_{a,i}\right)\right] \tag{7}$$

In Equation 7, n is the number of load increments to liquefaction; $\sigma_{d,i}$ and $\sigma_{d,i+1}$ are applied deviator stress at load increments "i" and "i+1", respectively; $\varepsilon_{a,i}$ and $\varepsilon_{a,i+1}$ are the axial strains at load increment "i" and "i+1", respectively.

In energy-based models, there is no need for definition of an equivalent number of cycles for introduction of a seismic action. With energy-based models, the stress or strain profile can be conveniently obtained based on the pore water pressure ratio (r_u)-cyclic shear strain (γ) relationship. One limitation of energy-based models is the need for information about complete stress-deformation history, which influences selection of convenient constitutive model [29]. However, under uniform and non-uniform loading conditions, the energy-based approach is a viable tool for evaluation of liquefaction [30-35]. Based on an experimental framework, Baziar et al. [36] developed a model to analyze strain energy-based liquefaction resistance based on parameters including initial effective overburden pressure, relative density and mean grain size. Xu et al. [37] also used the energy-based approach to analyze

the liquefaction potential of both loose and medium-density sand samples. Zhang et al. [38] performed a series of soil liquefaction tests and developed multivariate adaptive regression splines to find out the energy threshold triggering the liquefaction in sand and silt. Yang and Pan [39] studied cyclic resistance and pore water pressure generation in consolidated anisotropic sand samples using the Green, Mitchell and Polito Model (GMP) in conjunction with energy dissipation theory. Several experimental studies in the literature question the parameters affecting liquefaction behavior of silts and sands. Kokusho [40] evaluated the liquefaction potential of Futtsu sand using stress and energy-based methods with reference to varying relative densities and fines contents. Karakan et al. [32] performed cyclic triaxial tests on a non-plastic silt specimen of different relative densities. Varying cyclic strain levels were applied to observe the excess pore pressure development patterns, and also liquefaction behavior.

The residual pore pressures computed by the energy-based model and the experimental results are in good agreement. However, contrary to stress-based models, energy-based models do not require the conversion of randomized loads to an equivalent number of uniform load cycles. Moreover, the energy-based models are plausible alternatives to stress-based models for prediction of residual excess pore pressure generation patterns of cohesionless soils subjected to cyclic loading. Energy dissipation theory is a favorable tool in understanding the parameters influencing the liquefaction and pore water pressure generation behaviors in non-plastic silts. However, limited number of studies investigate the liquefaction phenomenon in pure non-plastic silts, based on energy-based models. In the present study, results of a series of stress-controlled consolidated undrained cyclic triaxial tests were analyzed to investigate the pattern and amount of dissipated energy threshold for the onset of liquefaction of a non-plastic silt. Relative density (D_r) and cyclic stress ratio (CSR) were determined to be the major influencing factors affecting the dissipated energy.

2. MATERIALS AND METHODS

2.1. Experimental Data

As mentioned before, results of cyclic triaxial tests performed by authors were used, and these studies report properties of non-plastic silt tested [32-33]. The specific gravity of non-plastic (NP) silt is 2.65 and the particle size distribution is given in Figure 1. The maximum and minimum void ratios in accordance with ASTM D4253 [41] and D4254 [42] standards were determined as 1.352 and 0.894, respectively. Cyclic triaxial tests were performed on samples prepared at six different relative densities ranging from 30% to 80%. For specimens prepared at different initial relative densities, 10 different cyclic triaxial tests of different CSRs were performed, which makes a total of 61 experiments (Data available in [32-33]).

Stress-controlled cyclic triaxial tests were performed to analyze the relationships among cyclic stress ratio (CSR), pore water pressure and double amplitude of axial strain. The device is equipped with a single column load frame, including a servo-pneumatic actuator with external displacement transducer. The servo-valve is able to apply a sinusoidal vibration frequency between 0.001 to 10 Hz. The device is capable of measuring axial displacement and load up to 50 mm. and 2 kN, respectively, by use of relevant transducers inside the cell. Volume change of specimens was measured by a double burette type volume change device, which is equipped with a transducer having a stroke of 25 ml (Figure 2).

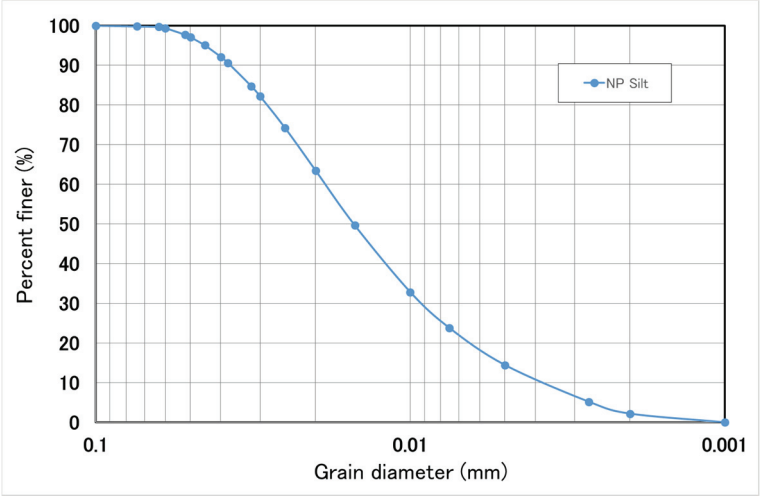

Figure 1 - Grain size distribution of non-plastic silt [45]

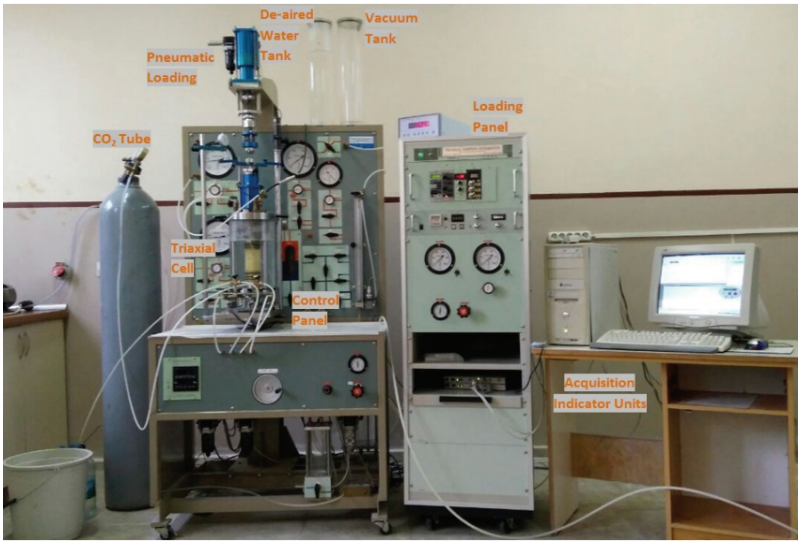

Figure 2 - Dynamic triaxial testing system

The tests were applied on specimens having dimensions of 50×100 mm (diameter×height), which were prepared and tested in accordance with JGS 0520-2000 and JGS 0541-2000 standards, respectively [43-44]. During specimen preparation, a vacuum of -20 kPa was applied to the specimen, in order to obtain a constant cross-sectional area throughout its height and prevent membrane penetration. Afterwards, the confining pressure was gradually increased as the vacuum pressure is also gradually decreased at a same rate. Later, carbon dioxide and de-aired water were circulated through the specimen. Saturation of specimens

were ensured by application of cell and back pressures. Consolidation under a confining pressure of 100 kPa was initiated after obtaining a Skempton's pore water pressure (B) value greater than 0.96. The next phase was application of undrained cyclic loading, and the liquefaction assessments were made until the specimens were exposed to 20 cycles of loading or when the double amplitude axial strain exceeds 5% [32]. During cyclic loading, excess pore water pressure, cyclic axial strain and cyclic deviator stresses were recorded simultaneously. After the loading stage, drainage valves are opened to drain the water in the soil sample. The water in soil specimen is transferred to volume change burette, enabling measurement of volume change due to post-liquefaction settlement. A series of tests on the required number of homogeneous specimens were performed, by gradually increasing the amplitude of cyclic load. Table 1 includes the details of the experiments including consolidation pressure, range of relative densities, CSR values, cyclic stress, pore water pressure ratios, volumetric strain, cyclic axial strain, double amplitude axial strain, factor of safety, number of tests and corresponding number of cycles to liquefaction. For providing a systematic approach, relative density of specimens was changed from 30% to 80%. Also, the specimens were subjected to different amplitudes of sine wave loading, by changing cyclic stress ratio (CSR) values. For specimens of 80% relative density, CSR values ranging between 0.173 and 0.226 caused higher strain levels up to 16%. Literally, a very low number of cycles between 0.5 to 1.5 caused liquefaction of silt, when subjected to higher CSR values. For 50% relative density, strain levels of specimens subjected to CSR values ranging between 0.149 and 0.186 are on the order of 12%. The specimens were completely liquefied after 2 to 7 cycles of loading, in other words, pore water pressure ratio has reached 100% and large strains were observed. For specimens having an initial relative density of 40%, strains corresponding to CSR values of 0.137 to 0.190 were approximately 9% whereas the soil lost its strength completely after 3 to 6 cycles. For specimens of 30% initial relative density, strains were recorded between 3.3% to 5% for CSR values between 0.123 and 0.166, with corresponding number of cycles from to 1 to 3.

In brief, the specimens, which were subjected to stress-controlled cyclic loading, were initially consolidated at 100 kPa under isotropic conditions. The dynamic loading pattern was a sine wave with a frequency of 0.1 Hz. As a result, excess pore water pressure (u), cyclic axial strain (ε_c), and cyclic deviatoric stresses were recorded continuously. Results of tests on a liquefied and a non-liquified sample are given in Figures 3 and 4, respectively. Here, the differences in stress path, change in stress path due to cyclic axial strain, and the change in number of cycles with pore water pressure ratio and cyclic axial strain by application of varying CSR levels on identical specimens of 60% relative density were presented. In this regard, a specimen of 60% relative density liquified after 13 cycles under a CSR value of 0.112 (Figure 3). In detail, Figure 3a presents the application of sine wave load of ±50 N for 13 cycles. Figure 3b shows the cyclic axial strain with number of cycles. It is evident that the specimen reaches 0.3%, 1.5% and 10% cyclic axial strains after application of 6, 11 and 12 cycles, respectively. Investigation of the change in pore water pressure with cyclic axial strains (Figure 3c), 6, 11 and 12 cycles come up with r_u values of 0.4, 0.65 and 0.75 and cyclic axial strains of 0.35%, 0.75% and 10%, respectively. Nevertheless, Figure 3d shows the variation of stress path, where maximum amplitude of principal stress difference is ±5.60 kPa. It is clearly observed that the mean effective stress of 100 kPa decreases to 0 after 13 cycles.

Table 1- Details of testing program

Test Number	Relative Density D_r (%)	Skempton value, B	Consolidation Pressure (kPa)	Cyclic Stress (kPa)	Cyclic stress ratio, CSR	Number of Cycles N	Pore Water Pressure Ratio	Cyclic Axial Strain $(\varepsilon_a)_{ss}$ (%)	Double amplitude of axial strain (%)	Cumulative $\sqrt{W_S}$	PEC	R^2	RMSE
0	80	1.00	99	2.18	0.011	20	0.02	0.009	0.018	Not liquified			
1	80	1.00	100	4.34	0.022	20	0.02	0.007	0.013	Not liquified			
2	80	1.00	99.8	8.31	0.042	20	0.04	0.019	0.039	Not liquified			
3	80	1.00	100	13.79	0.069	20	0.10	0.045	0.089	Not liquified			
4	80	1.00	99.6	20.13	0.101	20	0.23	0.086	0.173	Not liquified			
5	80	0.97	99.3	21.62	0.109	20	1.00	3.273	6.547	8.11	73.10	0.974	0.013
6	80	0.98	99.6	28.33	0.142	6	1.00	11.836	23.672	17.39	41.73	0.982	0.030
7	80	0.98	99.9	34.63	0.173	3	1.00	15.525	31.050	20.05	48.72	0.999	0.007
8	80	0.98	99.7	37.53	0.188	1.5	1.00	18.083	36.167	14.51	207.36	0.997	0.019
9	80	0.98	99.3	39.01	0.196	1	1.00	15.405	30.810	16.60	273.90	1.000	0.000
10	80	0.99	99.8	45.17	0.226	0.5	1.00	17.396	34.792	26.40	784.00	1.000	0.000
11	70	0.97	100	4.39	0.022	20	0.02	0.013	0.027	Not liquified			
12	70	0.99	99.6	9.32	0.047	20	0.06	0.019	0.039	Not liquified			
13	70	1.00	99.9	13.76	0.069	20	0.09	0.058	0.116	Not liquified			
14	70	1.00	98.9	17.24	0.087	20	0.23	0.127	0.254	Not liquified			
15	70	0.89	99	26.62	0.134	20	0.51	0.219	0.438	Not liquified			
16	70	0.98	99	29.00	0.146	6	1.00	11.060	22.120	9.48	31.14	0.994	0.014
17	70	0.94	99.2	34.26	0.173	3	1.00	14.565	29.130	8.99	37.45	0.991	0.027
18	70	0.98	99.2	37.73	0.190	1	1.00	11.962	23.924	16.08	284.93	0.999	0.016
19	70	1.00	100	40.31	0.202	0.8	1.00	18.053	36.106	25.53	748.57	0.022	0.997
20	70	1.00	99.5	41.26	0.207	0.5	1.00	18.046	36.092	25.21	635.04	1.000	0.000
21	60	0.98	99	4.45	0.022	20	0.03	0.016	0.031	Not liquified			
22	60	0.99	99.8	8.93	0.045	20	0.06	0.031	0.062	Not liquified			
23	60	1.00	99.5	13.79	0.069	20	0.14	0.074	0.147	Not liquified			
24	60	0.99	100	17.51	0.088	20	0.20	0.141	0.283	Not liquified			
25	60	1.00	100	21.67	0.108	13	1.00	9.101	18.202	6.73	48.44	0.987	0.012
26	60	0.90	100	25.61	0.128	3	1.00	11.944	23.889	16.28	16.00	0.975	0.043
27	60	0.97	99	34.47	0.174	1	0.90	7.221	14.441	11.60	70.56	0.996	0.036
28	60	1.00	99	38.24	0.193	0.7	1.00	8.922	17.843	13.08	171.61	1.000	0.001
29	60	1.00	98	42.51	0.217	0.5	1.00	10.021	20.041	14.15	198.81	1.000	0.000
30	60	1.00	99.9	37.88	0.190	0.8	1.00	18.085	36.171	23.72	561.69	1.000	0.000
31	50	1.00	99.2	2.21	0.011	20	0.01	0.011	0.022	Not liquified			
32	50	1.00	99	4.66	0.024	20	0.03	0.015	0.030	Not liquified			
33	50	1.00	99.6	9.46	0.048	20	0.06	0.031	0.061	Not liquified			
34	50	1.00	99.3	12.25	0.062	20	0.09	0.042	0.083	Not liquified			
35	50	0.90	99	13.82	0.070	20	0.08	0.056	0.113	Not liquified			
36	50	1.00	100	18.17	0.091	20	0.26	0.147	0.294	Not liquified			
37	50	1.00	100	23.64	0.118	18	1.00	7.109	14.218	9.16	58.22	0.980	0.036
38	50	1.00	99	29.55	0.149	7	1.00	11.616	23.232	11.59	38.32	0.990	0.040
39	50	0.93	99	32.26	0.163	5	1.00	12.733	25.466	18.35	121.00	0.983	0.025
40	50	1.00	99.6	36.95	0.186	2	1.00	11.534	23.067	17.97	30.36	1.000	0.020
41	40	1.00	100	2.16	0.011	20	0.02	0.012	0.023	Not liquified			
42	40	0.98	99.5	4.53	0.023	20	0.01	0.021	0.041	Not liquified			
43	40	1.00	99.9	9.47	0.047	20	0.06	0.029	0.058	Not liquified			
44	40	1.00	99.5	11.68	0.059	20	0.07	0.046	0.093	Not liquified			
45	40	1.00	99.7	13.99	0.070	20	0.09	0.059	0.118	Not liquified			
46	40	1.00	99.9	18.49	0.093	20	0.21	0.147	0.293	Not liquified			
47	40	0.99	99.5	24.65	0.124	20	0.46	0.306	0.612	Not liquified			
48	40	1.00	99.7	27.38	0.137	6	1.00	9.227	18.454	14.30	29.70	0.994	0.052
49	40	1.00	99.7	33.63	0.169	4	1.00	6.725	13.451	13.20	49.00	0.987	0.050
50	40	0.92	99.6	37.77	0.190	3	1.00	9.098	18.197	9.53	71.40	0.963	0.083
51	30	0.97	100	2.03	0.010	20	0.01	0.012	0.024	Not liquified			
52	30	0.97	99.8	4.46	0.022	20	0.02	0.020	0.041	Not liquified			
53	30	0.97	99.8	8.92	0.045	20	0.04	0.031	0.062	Not liquified			
54	30	1.00	99.9	11.37	0.057	20	0.07	0.046	0.092	Not liquified			
55	30	0.98	99.9	13.52	0.068	20	0.10	0.072	0.145	Not liquified			
56	30	0.96	100	17.42	0.087	20	0.35	0.188	0.376	Not liquified			
57	30	0.98	99.7	20.77	0.104	15	1.00	1.310	2.620	9.50	92.16	0.976	0.091
58	30	0.98	99.7	24.52	0.123	3	1.00	4.963	9.925	8.31	44.89	0.971	0.125
59	30	0.94	99.8	30.81	0.154	2	0.93	4.250	8.500	8.91	110.25	0.995	0.040
60	30	1.00	99.9	33.21	0.166	1	0.98	3.357	6.713	8.12	83.72	0.995	0.050

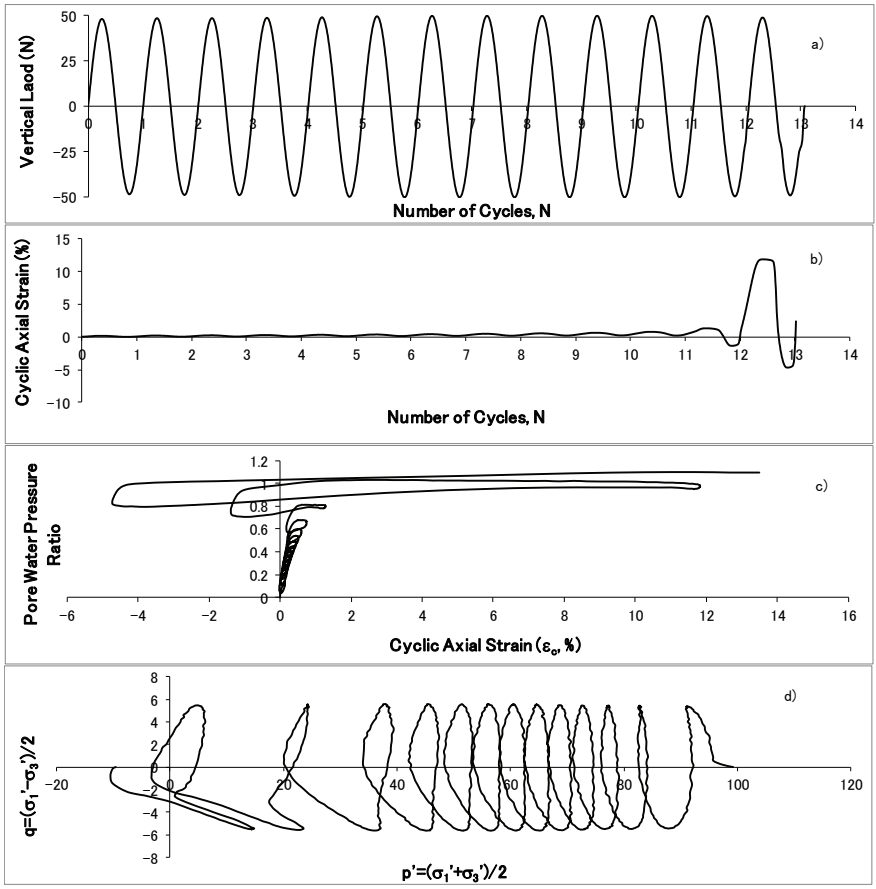

Figure 3 - Test results on a liquified specimen of 60% relative density under a CSR value of 0.112 (a) Change of sine wave load with number of cycles, (b) Change of cyclic axial strain with number of cycles, (c) Change of pore water pressure ratio with cyclic axial strain, (d) Stress path.

On the other hand, results of tests on a non-liquified specimen of 60% relative density are also shown in Figure 4. The specimen did not liquefy after 20 cycles under a CSR of 0.09, corresponding to a sine wave load of ±41 N. Figure 4b presents the variation of cyclic axial strain by number of cycles. Strictly speaking, the strains reach to 0.28%, after 20 cycles of loading. The non-liquified specimen reaches a pore water pressure ratio and axial strain of 0.25 and 0.28%, respectively (Figure 4c). Finally, Figure 4d shows the variation of stress path, where maximum amplitude of principal stress difference is ±4.50 kPa. It is evident that the mean effective stress of 100 kPa decreases by a relatively small value, down to 82 kPa.

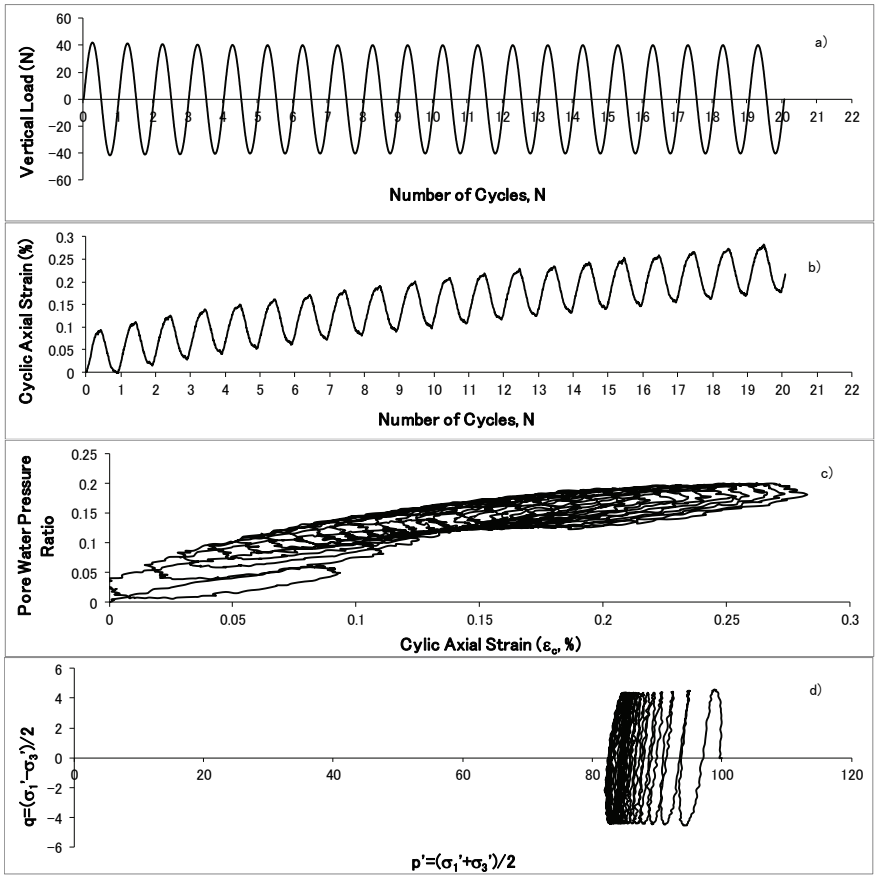

Figure 4 - Test results on a non-liquified specimen of 60% relative density under a CSR value of 0.09 (a) Change of sine wave load with number of cycles, (b) Change of cyclic axial strain with number of cycles, (c) Change of pore water pressure ratio with cyclic axial strain, (d) Stress path.

2.2. Calculation of Energy Dissipated Per Unit Volume

The method proposed by Green et al. [7], which is previously introduced in "Introduction" was used as a guide. The analyses were employed on liquified test results, which are presented in Table 1. In this regard, the energy-based pore water pressure calculation procedure was not applied for 33 non-liquified tests. For example, for 80% relative density, in experiment #3 in Table 1, for CSR=0.069 after 20 cycles, the PWP was 10.28%, while in experiment #4 for CSR=0.101 after 20 cycles, the PWP was 22.89%. These values clearly demonstrate that liquefaction did not occur in these tests.

The change in excess pore water pressure corresponding to energy absorbed per unit volume (W_s) for a certain loading cycle can be calculated by use of the calculating the ratio of energy

dissipated per unit soil volume to the initial average effective stress. Defined in Equation (3), physical meaning of W_s is given in Figure 5.

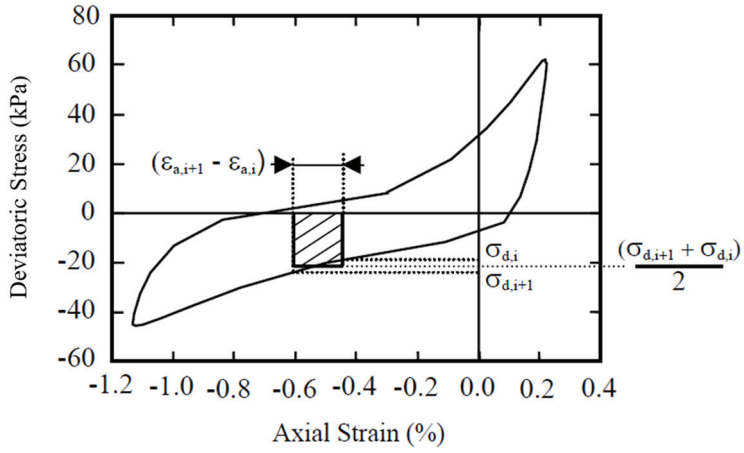

Figure 5 - Hysteresis loop of a cycle as a result of cyclic loading [7]

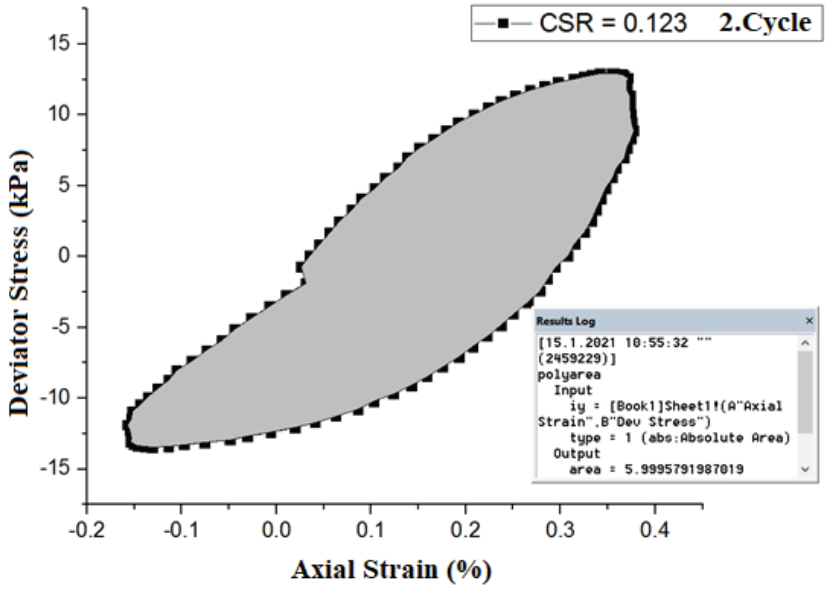

Figure 6 - Calculation of the hysteresis loop area in 2nd cycle of Test #58 with CSR = 0.123

During cyclic loading, the energy consumed per unit volume for a soil sample is defined as the area covered a by deviatoric stress-strain hysteresis cycle [7]. In a certain test, a hysteresis

loop corresponding to each cycle is drawn, and the energy consumed (W_s) in that cycle is the area limited by the relevant cycle. Therefore, the variation of deviatoric stress by axial strain were plotted for each cycle. The areas covered by certain cycles in deviatoric stress-axial strain plots were calculated. An example of the hysteresis loop area calculation is shown in Figure 6.

2.3. Pseudo Energy Capacity (PEC) Calculations

The pseudo-energy capacity (calibration parameter) calculation called PEC is as important as the W_s (energy consumed) in the r_u formulation given in Equation (1) as shown in Figure 7.

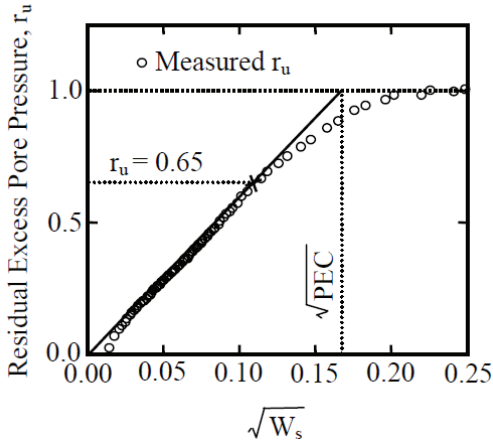

Figure 7 - An illustration of determination of PEC from dynamic triaxial test results [7].

To determine the PEC value of each experiment, first of all, $\sqrt{W_s}$ from each cycle are cumulatively calculated and plotted in abscissa (Figure 8).

Afterwards, experimental r_u value at the end of the relevant cycle is plotted on ordinate and the variation of r_u with $\sqrt{W_s}$ is obtained. A line is drawn (dashed line) from r_u = 0.65, intersecting the curve formed by the resulting r_u - $\sqrt{W_s}$ data. Next, the red line in the figure is drawn, between the origin and the curve, corresponding to a r_u value of 0.65. Finally, this red line is extended to the the horizontal line of r_u = 1.00 and the abscissa of the intersection of these two lines is $\sqrt{PEC}$. Calculated PEC values are given in Table 1. Numerically, this procedure simplifies to Equation 8:

$$PEC = \frac{W_{s,r_u=0.65}}{0.4225} \tag{8}$$

where $W_{s,ru=0.65}$ is the value of W_s corresponding to r_u = 0.65. The term “pseudo energy capacity” or PEC is used to label the calibration parameter to give a certain amount of

physical significance to it over just a general curve fit parameter. PEC is approximately equal to the energy dissipated per unit volume normalized by the initial effective confining pressure in a sample up to the point of initial liquefaction.

Afterwards, W_s and PEC values were substituted in Equation 1 to calculate r_u values. Lastly, experimental and calculated pore water pressure ratio (r_u) values were plotted against number of cycles (N).

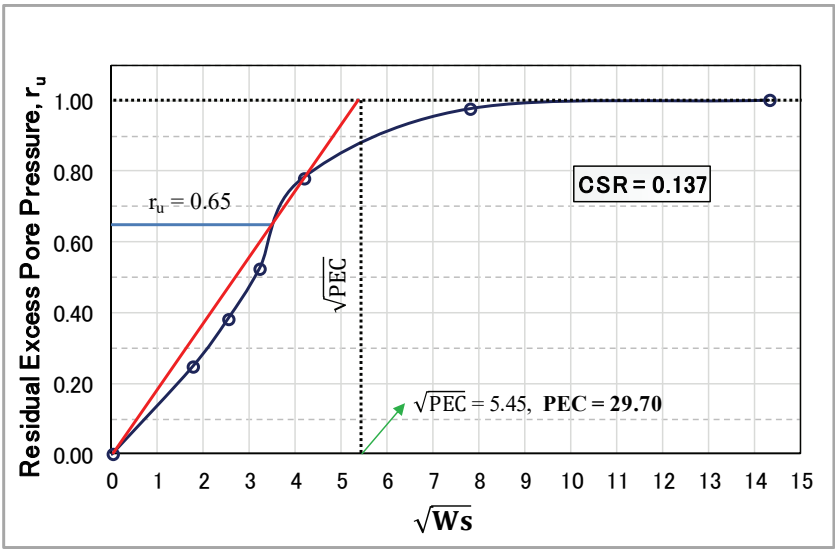

Figure 8 - A sample PEC calculation for CSR = 0.137

3. RESULTS AND DISCUSSION

Using the procedure explained above, application of energy-based pore water pressure models for sands on evaluation of pore water pressure development behavior of non-plastic silts were analyzed. Figure 9 shows the pore water pressure ratio (r_u) – number of cycles (N) relationship for a test with cyclic stress ratio (CSR) *of* 0.119 at a relative density (D_r) of 50%. As can be observed, with increasing number of cycles, modeled r_u values reaches 1 after application of approximately 17 cycles. As can be observed, with increasing number of cycles, modeled r_u values reach to 1 after approximately 16.5 cycles. However, experimental data show that same r_u value was obtained after 17th cycle.

3.1. Comparison of calculated and experimental r_u values

The relationship between pore water pressure ratio (r_u) and number of cycles (N) for liquefied tests on specimens with relative densities ranging between 30% to 80% are given in Figure 10. Analyzing results of test performed under a CSR of 0.104, while the energy based r_u values were higher than experimentally obtained r_u values until the 14th cycle, it is clear that

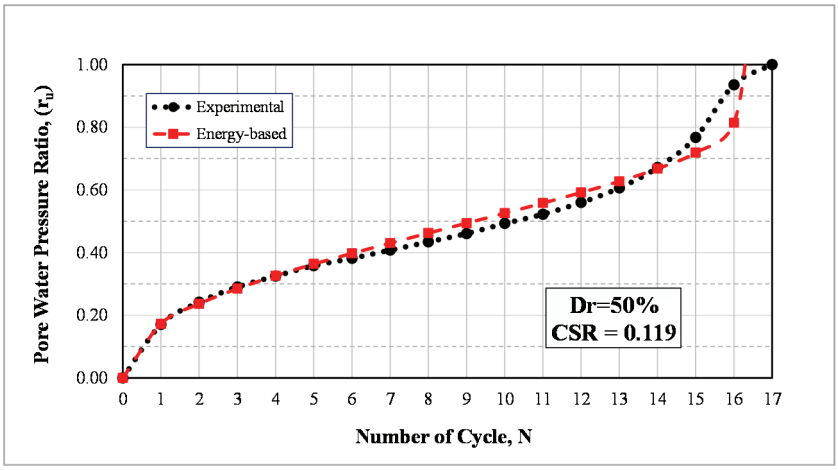

Figure 9 - An example of comparison of experimental and energy-based r_u values.

the r_u values converge from 14th to 15.2nd cycle (Figure 10a). When CSR was increased to 0.123, it is observed that the modeled r_u value reaches 1 after 2.6 cycles, while the experimental r_u value reaches 1 at the end of the 3rd cycle. Under a CSR of 0.154, it is understood that the experimental r_u value can rise up to 0.93 and liquefaction is evident, while the model results show that soil liquefies at an r_u value of 1. Similarly, the maximum of modeled r_u value for CSR = 0.166 is determined to be 0.88-which is also experienced in reality (Figure 10a). As seen in Figure 10a, for D_r = 30%, the number of cycles required for r_u to reach 1.0 decreased as the CSR value increased. For instance, the number of cycles required for liquefaction for CSR values of 0.166 and 0.104 are 1 and 15, respectively.

Considering results of test of CSR = 0.137, it is observed that the onset of liquefaction is at 2nd cycle during the experiment, and the model shows that the specimen liquifies at 1.7th cycle. For CSR = 0.168, liquefaction is observed after 4th and 3.2nd cycle, according to experimental and model outcomes (Figure 10b). Likewise, for CSR = 0.190, although it is seen that it liquefied after 5.1st cycle in reality, modeling results show that the soil liquefied after 4.5th cycle (Figure 10b).

Analyzing results obtained from liquefied tests on specimens of D_r=50%, although r_u value calculated as a result of the energy-based analysis in all four liquefied tests shows a similar trend with experimental results, it is seen that the model outcomes show liquefaction before experimental outcomes (Figure 10c). Although it is found that the modeled r_u value in the CSR = 0.119 test reached 1 in the 16.5th cycle, in reality, it is evident that the soil liquefies after 17th cycle. For CSR = 0.149, r_u value increased up to 1 after 6 cycles, model outcomes state that r_u increased up to 1 after 5.2 cycles. In tests with CSR = 0.163 and CSR = 0.183, experimental and modeled r_u values rise to 1, and the model and real behaviors are in agreement with each other. In Figure 10c, analyzing behavior of specimen of D_r = 50%, for CSR = 0.183, the pore water pressure ratio reaches 1.00 after just one cycle.

Focusing on Figure 10d, for CSR = 0.112, liquefaction is initiated after 12th cycle and the model outcomes show that r_u value reaches 0.97 after same number of cycles. At CSR =

0.131, the experimental and model results show that the r_u value reaches 1 after 3rd and 2.1st cycles, respectively. At CSR = 0.172, while it is observed that the experimental r_u value reaches a level of 0.90 and liquefies in the 1.27th cycle, it is calculated that modeled r_u values reach to 1.0 even after 1.15th cycle. In the three liquefied tests with CSR values greater than 0.172, the r_u values found as a result of the experimental and energy-based analysis follow a similar trend, and liquefied around 1st cycle. In Figure 10d, the number of cycles required for the r_u to reach 1.0 for both CSR = 0.217 and CSR = 0.193 has been determined as 1. When CSR = 0.172, the number of cycles required for the r_u to reach 1.00 is just over 1. For all three liquefied specimens with D_r=70% and applied CSR greater than 0.188; the number of cycles in which r_u values reaches 1.0 were same for energy-based model and experimental outcomes (Figure 10e). For D_r = 70%, the number of cycles required for r_u to reach 1.0 for CSR values of 0.211, 0.208 and 0.194 are equal to 1. In this case, as the CSR value increases with the increasing relative density, it was shown that one cycle is sufficient when the number of cycles required for liquefaction exceeds a certain CSR value.

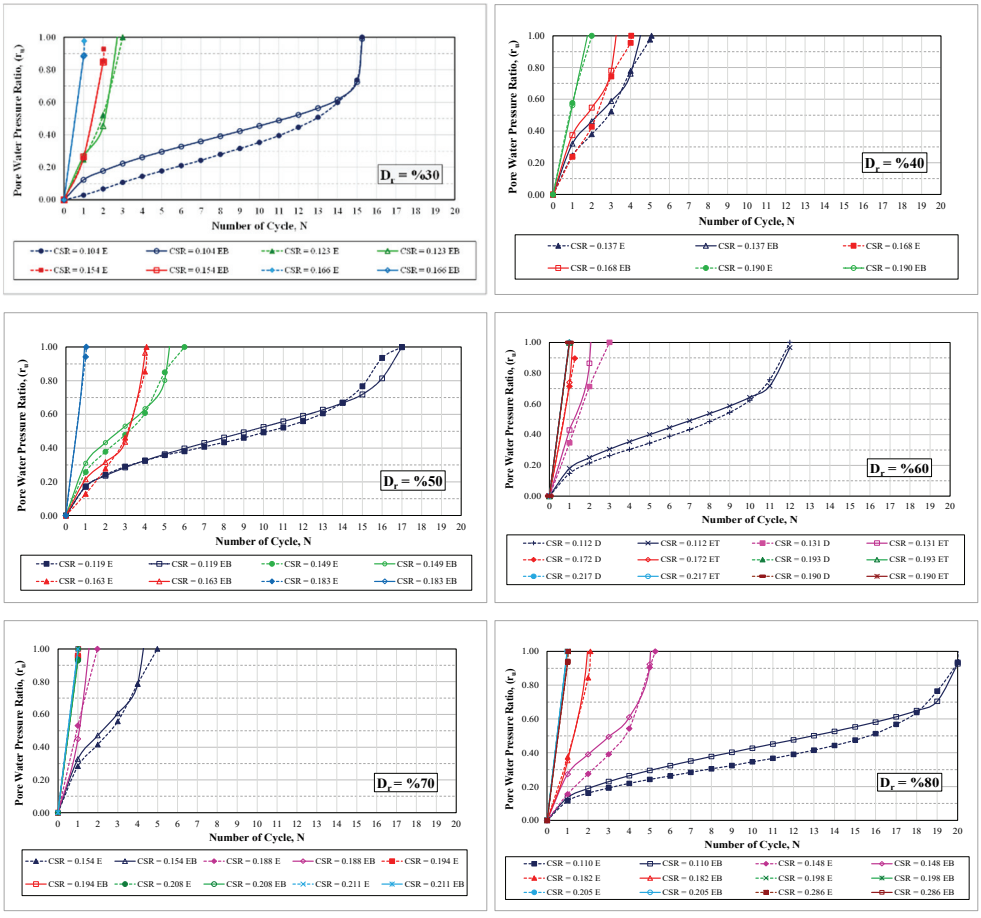

Figure 10- The relationship between r_u and number of cycles - liquefied tests with D_r=30% to 80% (E = Experimental, EB = Energy-based)

Results of test performed under CSR = 0.110 revealed that the r_u value escalated up to 1 in the 20.1st cycle (Figure 10f). However, energy-based analysis concludes that the real r_u value reaches a maximum of 0.95 in the relevant cycle, and liquefaction is initiated. At a CSR of 0.148, while the r_u value reached 1 in the 5.27th cycle during testing, model outcomes reveal that r_u value reaches 1 after 5 cycles. For a CSR of 0.182; r_u reached 1 after 2.11 cycles, while in the model outcomes, a value of 1 is reached after 1.95 cycles. When CSR exceeds 0.182, all three specimens of D_r=80% liquefied in the first cycle, and the model outcomes are in accordance with experimental values. For dense specimens, when CSR is above 0.198, the number of cycles needed for liquefaction is less than 1. At a constant CSR value, the number of cycles required for liquefaction and pore water pressure ratio increased with increasing relative density values.

3.2. Dependence of Cumulative $\sqrt{W_s}$ on r_u Values

In Figure 11, for six relative density values ranging from 30% to 80%, the variation of cumulative √(Ws) at different CSR values with pore water pressure ratios was obtained. For loose specimens, at smaller CSR amplitudes, increasing number of cycles causes a stepwise increase $\sqrt{W_s}$ values, causing r_u values ascend to 1. Nevertheless, results of four experiments in Figure 11 show different trends from those of the rest. In detail, the first test of Dr=60% and CSR=0.190 liquified after one single cycle, and √(Ws) is calculated as 23.72. In the next two tests on specimens with a D_r value of 70%, under CSRs of 0.211 and 0.208, number of cycles required to initiate liquefaction are 1 and 1.3, respectively. Corresponding √(Ws) values are 25.20 and 25.53, respectively. In the fourth test, a high CSR value of 0.286 was applied on specimen of highest relative density (Dr=80%), it expectedly liquified after one cycle, and the √(Ws) value was calculated as 26.40. Considering common aspects of the last four tests, high CSR values caused liquefaction of dense to very dense specimens after very low number of cycles.

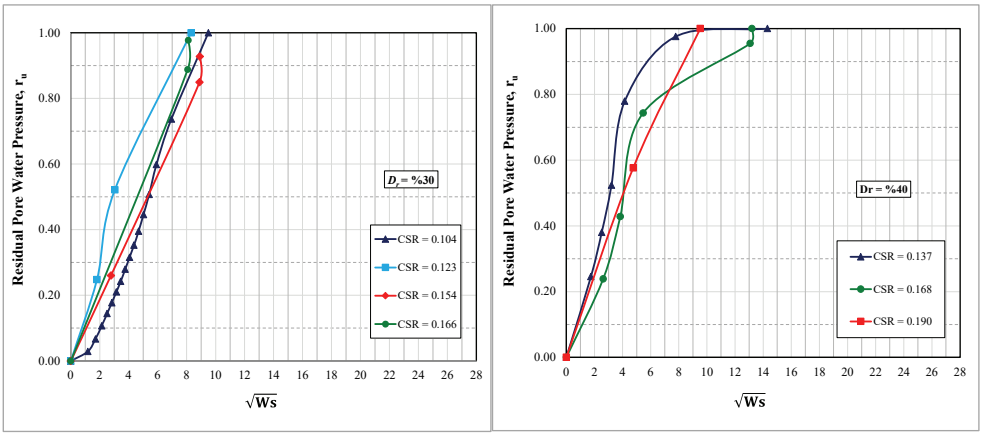

Figure 11- The relationship between pore water pressure ratio and cumulative number √Ws for liquefied tests with relative densities ranging between 30% to 80% and varying CSR

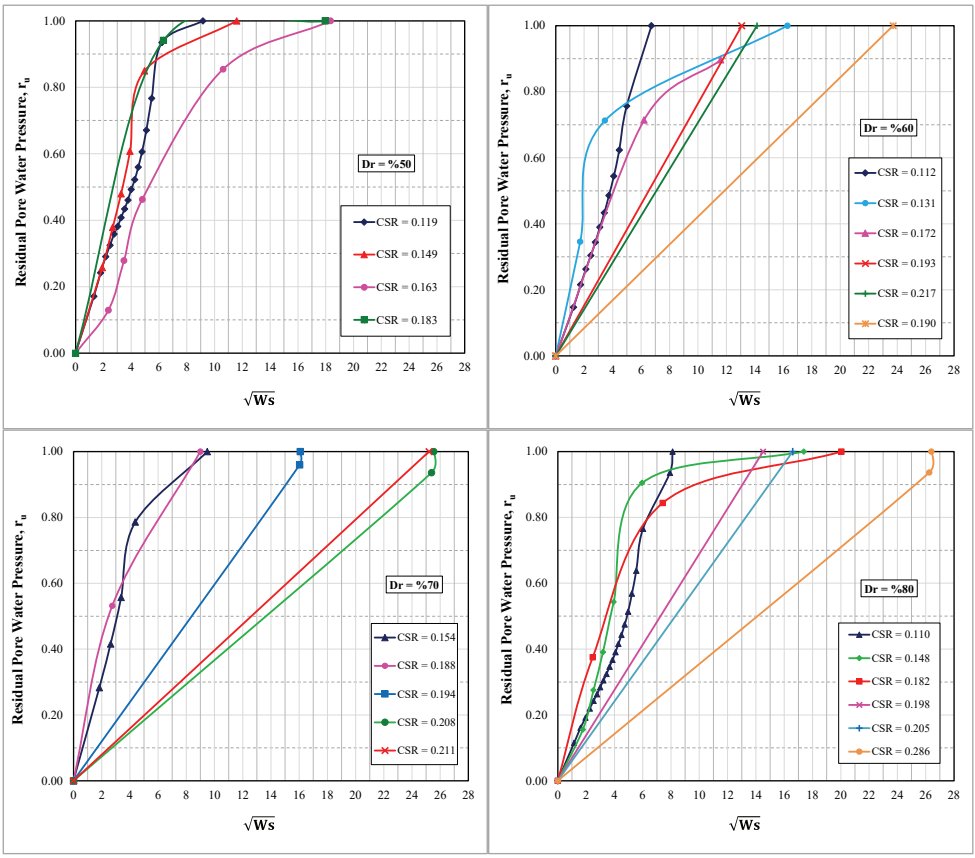

Figure 11- The relationship between pore water pressure ratio and cumulative number √Ws for liquefied tests with relative densities ranging between 30% to 80% and varying CSR (continued)

3.3. Variations of Accumulative Dissipated energy with the Number of Cycles

According to Yang and Pan [39] and Kokusho [40] and the dissipated energy (W_s) during cyclic undrained loading can be calculated by finding the hysteretic area of each individual stress–strain loop. In Figure 12, change of W_s by increasing N by increasing CSR is presented for a wide range of relative densities, starting from 30% to 80%. As shown in Figure 12a, when the non-plastic silt is at a very loose state, accumulated energy after 15 cycles is 0.483 kJ/m^3. Further increase in CSR decreased number of cycles below 2, and corresponding accumulated energy is between 0.6 and 0.8 kJ/m^3. When D_r=40% and CSR=0.137, accumulated energy after 5 cycles is 2.045 kJ/m^3 (Figure 12b). For medium dense specimens (D_r=50% and 60%), similar behaviors were observed. For instance, when CSR=0.119, while 17 cycles cause accumulation of an energy of 0.84 kJ/m^3 (Figure 12c), 12 cycles under a CSR of 0.112 accumulate an energy of 0.45 kJ/m^3 (Figure 12d). Without hesitation, increasing CSR caused decrease in number of cycles, while increasing accumulated energy at this

density level. For dense specimens (Dr=70%), high CSR values of 0.211 and 0.208 caused liquefaction before one single cycle and accumulated energy was calculated as 6.40 and 7.50 kJ/m^3 (Figure 12e). At densest state, six CSR levels were applied ranging from 0.110 to 0.286. Accumulated energy for CSR of 0.110 after 20 cycles and CSR of 0.286 after one cycle were obtained as 0.628 and 6.89 kJ/m^3.

Figure 12 presents the variation in the accumulative dissipated energy with *N* for typical tests for relative densities ranging from 30% to 80%. For the nonplastic silt under isotropic consolidation, Figures 12(a) to 12(f) shows that the energy accumulation is insignificant at the beginning but accelerates when the cyclic strain starts to develop rapidly for CSR=0.183 (Figure 12c) and reaches a value of 3.28 kJ/m^3 when cyclic failure occurs with 5% double amplitude axial strain. In Fig. 11d, although a larger energy dissipation is required for failure for D_r=60% (W_f = 4.018 kJ/m^3), *W–N* relationship exhibits a similar upward concave tendency as that of dense samples (Dr=70% and 80%).

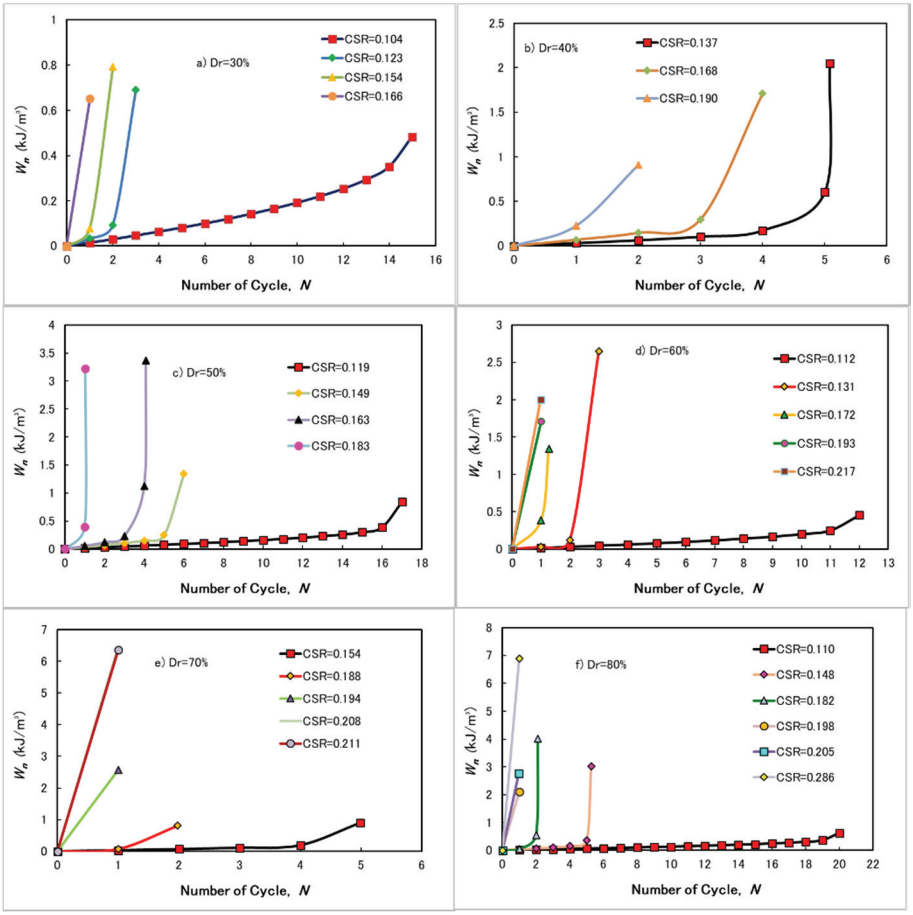

Figure 12 - Variations of accumulative dissipated energy with the number of cycles for 30% to 80% relative densities and different CSR values

The constraints of the model are limited by the conditions enlisted in Table 1. A wide range of relative densities from 30% to 80% were used, use of relative density values out of this range is inconvenient. The soil is a commercially available silt, which is free of coarse-grained content. These results cannot be used for modeling silt behavior of different plasticity levels. For each relative density, the tests were initiated by selecting a very small CSR value and then the cyclic stress ratio was gradually increased until number of cycles to liquefaction drops to one. Thus, the variation of CSR values could be analyzed in a very wide range. About the potential sources of error, calculation of area covered by deviatoric stress-axial strain plot is not prone to errors. However, the empirical approach for calculation of PEC can be discussed. Since it is empirical, we found that this approach can be used for evaluation of pore pressure development pattern of silts. Therefore, sources of error in modeling can be associated with PEC value, further studies can discuss the method for obtaining PEC, by performing cyclic tests on different types of soils. The changes in coefficient of determination (R^2) and root mean square error (RMSE) values for each modeling attempt is calculated and tabulated in Table 1. Analyzing the results, it is observed that the performance of model is higher for increasing CSR values, which can be observed by decreasing RMSE and increasing R^2 values, regardless of the relative density (D_r) value.

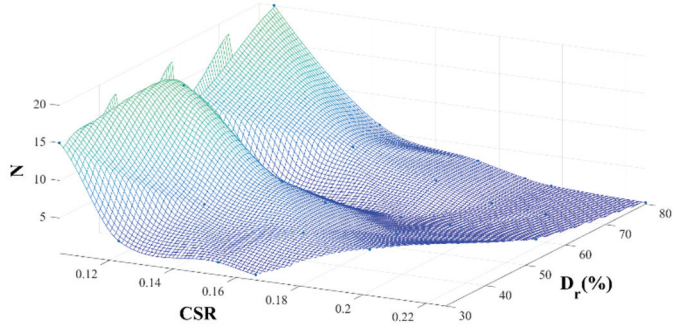

(a)

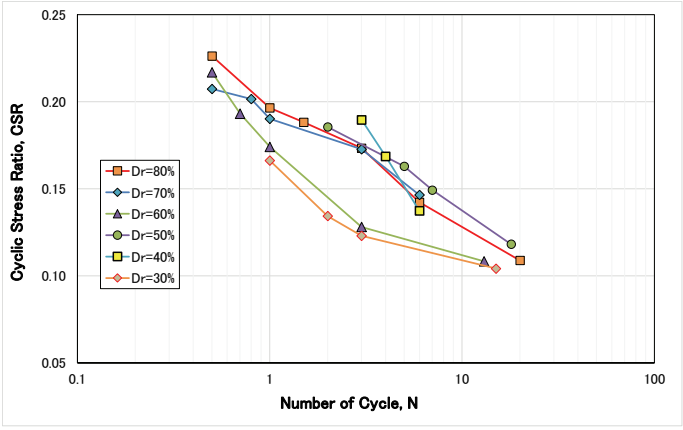

(b)

Figure 13 - a) Variation of number of cycles to liquefaction with varying CSR and D_r b) Biaxial representation of data

Lastly, Figure 13a presents a 3D plot of CSR, D_r and N. It is clear that at lower relative density and higher CSR values, the specimen liquifies after a lower number of cycles. On the other hand, it was also observed that, for a certain CSR value, increasing relative density causes an increase in number of cycles to liquefaction. Figure 13b also show that as the cyclic stress ratio increases for any sample, the number of cycles to reach initial liquefaction decreases.

5. CONCLUSIONS

In this study, the applicability of a previously proposed energy-based model for analysis of the pore pressure development in sands on a nonplastic silt was questioned. In this regard, by use of a previously published data set consisting of 61 cyclic triaxial test results was utilized. The tests were performed at 6 different relative densities (D_r) *ranging from 30% to 80%* and 10 different cyclic stress amplitude ratios (CSR). In the current energy-based model, the key parameters of pore water pressure development and shear deformation were determined as relative density, cyclic stress ratio and number of cycles. In order to analyze these behaviors, areas covered by 852 deviator stress–axial strain hysteresis loops of from these tests were calculated. After calculation of area, PEC (Pseudo Energy Capacity) values were obtained in order to calculate the energy-based pore water pressure ratio (r_u). Afterwards, the variation of pore water pressure ratio with number of cycles in 28 liquefied test were obtained and comparative pore water pressure – number of cycle plots of liquefied tests at each relative density were presented. Following conclusions can be drawn from this study:

- The energy-based pore pressure behavior models proposed so far were mostly applied for analysis of dynamic test results on clean sands. Applying the model by use of test results on non-plastic silt specimens (28 liquefied tests from a total of 61), the concordance among the model outcomes and experimental r_u values were provided.
- In 28 liquified tests, the model-based development pattern of energy-based pore pressure ratios were in a similar trend with experimental records.
- In 50% (14/28) of the specimens liquefied, the modeled r_u values reached 1 at lower number of cycles, compared to experimental outcomes.
- When liquefied experiments with six different relative densities were examined; particularly the specimens liquefied within the first cycle, the number of cycles in real and model outcomes to reach a value of $r_u = 1$ are approximately the same. For this reason, a comparison of the experimental and energy-based r_u revealed that, differences between the number of cycles to reach liquefaction state was not remarkable. However, the performance of energy-based model was better for samples liquefied after 1 cycle. It should be noted that, the specimens liquefied in earlier number of cycles, with reference to the experimental records.
- As the CSR values are reduced, it is observed that the modeling ability of energy-based model is increased.

- The energy-based pore pressure development model, which was previously proposed for clean sand soils, can be reliably applied to analyze behavior of non-plastic silts.
- Methods of estimating pore water pressure with constitutive models require a large number of input parameters that are not easy to determine in the absence of advanced laboratory test results. For this reason, it is thought that empirical or semi-empirical models will be used more widely for a while. However, in cases where laboratory test results are sufficient, energy-based pore pressure calculation yields very efficient results.
- The limitation of energy-based pore pressure modeling is that the test data should be firm, and the entire stress-strain history of specimens should be known. However, the advantage of energy-based studies is that there is no need to convert the earthquake wave motion to equivalent number of cycles in stress-based studies.
- Analyzing past studies, it was observed that experimental efforts are concentrated on testing clean sands and sand-silt mixtures. This study demonstrates that the energy-based pore water pressure model can also be used to simulate the pore pressure generation behavior of non-plastic silts. Comparison of the test results with model outcomes reveal that energy-based pore water pressure models are viable tools for simulation of pore water pressure development pattern of non-plastic silts, within a certain confidence interval. It should be emphasized that use of the model is limited to only non-plastic silts, more effort is needed to prove the applicability of method to a wide range of grain sizes, shapes, size distributions and plasticity indices.

References

[1] Kramer, S. L., Geotechnical earthquake engineering, Prentice-Hall Civil Engineering and Engineering Mechanics Series, Upper Saddle River, NJ: Prentice Hall. 1996.

[2] Towhata, I., Geotechnical earthquake engineering. Berlin Heidelberg: Springer – Verlag, 2008.

[3] Amini, P. F., and Noorzad, R., Energy based evaluation of liquefaction of fiber-reinforced sand using cyclic triaxial testing. Soil Dynamics and Earthquake Engineering, 104, 2018.

[4] Scott, R. F., Principles of soil mechanics, Addison-Wesley, Reading, Mass. 1963.

[5] Lambe, T. W., and Whitman, R. V., Soil mechanics, Wiley, New York. 1969.

[6] Dobry, R., Ladd, R. S., Yokel, F. Y., Chung, R. M., and Powell, D., Prediction of pore-water pressure buildup and liquefaction of sands during earthquakes by the cyclic strain method. National Bureau of Standards Building Science Series 138, National Bureau of Standards, U.S. Dept. of Commerce, Washington, D.C. 1982.

[7] Green, R. A., Mitchell, J. K., and Polito, C. P., An energy-based excess pore-water pressure generation model for cohesionless soils. Proc., John Booker Memorial Symp.-Developments in Theoretical Geomechanics, D. W. Smith and J. P. Carter, eds., Balkema, Rotterdam, Netherlands, 383–390, 2000.

[8] Seed, H.B., Martin, P.P., and Lysmer, J. (1975). The generation and dissipation of pore water pressures during soil liquefaction. Rep. No. EERC 75-26, Univ. of California, Berkeley.

[9] Booker, J.R., Rahman, M.S., and Seed, H.B. (1976). GADFLEA—A computer program for the analysis of pore pressure generation and dissipation during cyclic or earthquake loading. Rep. No. EERC 76-24, Earthquake Engineering Research Center, Univ. of California at Berkeley, Berkeley, California.

[10] Dobry, R., Ladd, R., Yokel, F., Chung, R., and Powell, D. (1982). Prediction of pore water pressure buildup and liquefaction of sands during earthquakes by the cyclic strain method. NBS Building Science Series 138, National Bureau of Standards, U.S. Dept. of Commerce.

[11] Cetin K.O, and Bilge, H.T. (2012). Cyclic Large Strain and Induced Pore Pressure Models for Saturated Clean Sands. Journal of Geotechnical and Geoenvironmental Engineering, 138 (3).

[12] Jafarian Y, Towhata I., Baziar M.H., Noorzad A. and Bahmanpour A., (2012). Strain energy based evaluation of liquefaction and residual pore water pressure in sands using cyclic torsional shear experiments. Soil Dynamics and Earthquake Engineering. 35, 13–28.

[13] Elgamal, A., Yang, Z., Parra, E. and Ragheb, A. (2003). Modeling of cyclic mobility in saturated cohesionless soils. Int. J. Plast., 19(6), pp. 883–905.

[14] Polito, C.P., Green, R.A., and Lee, J. (2008). Pore pressure generation models for sands and silty soils subjected to cyclic loading. J. Geotech. Geoenviron. Eng., 134(10), 1490–1500.

[15] Baziar M.H., Shahnazari H., and Sharafi H., (2011). A laboratory study on the pore pressure generation model for Firouzkooh silty sands using hollow torsional test International Journal of Civil Engineering, 9 (2).

[16] Lee, K., and Albaisa, A. (1974). Earthquake induced settlements in saturated sands. J. Geotech. Eng. Div., 100(4), 387–405.

[17] De Alba, P., Chan, C.K., and Seed, H.B. (1975). Determination of soil liquefaction characteristics by large scale laboratory tests. EERC Rep. No. 75-14, Univ. of California, Berkeley, CA.

[18] Seed, H.B. and Lundgren R. "Investigation or the effect or transient loading on the strength and deformation characteristics of saturated sands",· Proc ASTM, vol. 54, pp 1288-1306.

[19] Seed, H.B. and Fead, J.W.N. (1959) "Apparatus for Repeated Load Tests on Soils" Special Technical Publication No 204 ASTM Philadelphia.

[20] Seed, H.B. (1960). Soil Strength During Earthquakes, Proceedings of World Conference of Earthquake Engineering, vol I, pp 183-194.

[21] Nemat-Nasser, S., and Shokooh, A., A unified approach to densification and liquefaction of cohesionless sand in cyclic shearing. Can. Geotech. J., 16(4), 1979.

[22] Davis, R. O., and Berrill, J. B., Energy dissipation and seismic liquefaction in sands. Earthquake Eng. Struct. Dyn., 10(1), 1982.

[23] Davis, R. O., and Berrill, J. B., Pore pressure and dissipated energy in earthquakes—Field verification. J. Geotech. Geoenviron. Eng., 127(3), 2001.

[24] Yamazaki, F., Towhata, I., and Ishihara, K., Numerical model for liquefaction problem under multi-directional shearing on horizontal plane. Proc., 5th Int. Conf. on Numerical Methods in Geomechanics, Vol. 1, Taylor & Francis Group, London, 1985.

[25] Law, K. T., Cao, Y. L., and He, G. N., An energy approach for assessing seismic liquefaction potential. Can. Geotech. J., 27(3), 1990.

[26] Hsu, H. L., Study on the relationship between shear work and pore-water pressure for saturated sand in undrained test. First Int. Conf. on Earthquake Geotechnical Engineering, K. Ishihara, ed., Vol. 1, Balkema, Rotterdam, Netherlands, 1995.

[27] Wang, G. J., Takemura, J., and Kuwano, J., Evaluation of excess pore-water pressures of intermediate soils due to cyclic loading by energy method. Computer methods and advances in geomechanics, J. X. Yuan, ed., Balkema, Rotterdam, Netherlands, 1997.

[28] Green, R. A., Energy-based evaluation and remediation of liquefiable soils. Ph.D. dissertation, Civil Engineering, Virginia Polytechnic Institute and State Univ., Blacksburg, VA, 2001.

[29] Cetin, K. O., and Bilge, H. T., Cyclic large strain and induced pore pressure models for saturated clean sands. Journal of Geotechnical Geoenvironmental Engineering. 2012.

[30] Polito, C., Green, R. A., Dillon, E., Sohn, C., Effect of load shape on relationship between dissipated energy and residual excess pore pressure generation in cyclic triaxial tests. Can Geotech J. 50(11):1118–28, 2013.

[31] Azeiteiro, R.J.N. Coelho, P. A. L. F., Taborda, D. M. G., Grazina, J. C. D., Energy based evaluation of liquefaction potential under non-uniform cyclic loading. Soil Dynam Earthq Eng. 92:650–65, 2017.

[32] Karakan, E., Tanrınıan, N., and Sezer A., Cyclic undrained behavior and post liquefaction settlement of a nonplastic silt, Soil Dynamics and Earthquake Engineering, 120, 2019a.

[33] Karakan, E., Sezer A., and Tanrınıan N., Evaluation of effect of limited pore water pressure development on cyclic behavior of a nonplastic silt, Soils and Foundations, 59(5), 2019b.

[34] Pan, K., Yang, Z. X., Evaluation of the liquefaction potential of sand under random loading conditions: equivalent approach versus energy-based method. Journal of earthquake engineering. 24 (1) :59–83.2020.

[35] Karakan, E., Validation of pore water pressure model calibration parameters for non-plastic silt. *Fresenius environmental bulletin*, *29*(12), 2020.

[36] Baziar, M.H., Sharafi, H., Assessment of silty sand liquefaction potential using hollow torsional tests—an energy approach. Soil Dynam Earthq Eng. 31(7), 2011.

[37] Xu, C., Feng, C., Du, X., Zhang, X., Study on liquefaction mechanism of saturated sand considering stress redistribution. Engineering Geology. 264, 2020.

[38] Zhang, W., Goh, A., Zhang, Y. M., Chen, Y. M., Xiao, Y., Assessment of soil liquefaction based on capacity energy concept and multivariate adaptive regression splines. Eng Geol. 188:29–37, 2015.

[39] Yang, Z. X., Pan, K., Energy-based approach to quantify cyclic resistance and pore pressure generation in anisotropically consolidated sand. J Mater Civ Eng. 30 (9), 2018.

[40] Kokusho T., Liquefaction potential evaluations: energy-based method versus stress based method. Can Geotech J 2013;50(10) 2013.

[41] ASTM, Standard Test Methods for Maximum Index Density and Unit Weight of Soils Using a Vibratory Table: D4253-16e1, American Society for Testing and Materials, 14p. 2016.

[42] ASTM, Standard Test Methods for Minimum Index Density and Unit Weight of Soils and Calculation of Relative Density: D4254-16, American Society for Testing and Materials, 9p. 2016.

[43] JGS 0520-2000, Preparation of Soil Specimens for Triaxial Tests.

[44] JGS 0541-2000, Method for Cyclic Undrained Triaxial Test on Soils.

[45] Tanrınıan, N., Post-Liquefaction Settlement Behavior of Non-Plastic Silts, Master Thesis, Ege University, İzmir. 2018.